Geophysical Research Letters

RESEARCH LETTER
10.1029/2024GL109251

Contrasting Response of Mesoscale Convective Systems Occurrence Over Tropical Land and Ocean to Increased Sea Surface Temperature

Wenhao Dong[1,2], Ming Zhao[2], Lucas Harris[2], Kai-Yuan Cheng[3], Linjiong Zhou[3], and V. Ramaswamy[2]

[1]Cooperative Programs for the Advancement of Earth System Science, University Corporation for Atmospheric Research, Boulder, CO, USA, [2]NOAA/Geophysical Fluid Dynamics Laboratory, Princeton, NJ, USA, [3]Program in Atmospheric and Oceanic Sciences, Princeton University, Princeton, NJ, USA

Abstract Mesoscale convective systems (MCSs) are pivotal in global energy/water cycles and typically produce extreme weather events. Despite their importance, our understanding of their future change remains limited, largely due to inadequate representation in current climate models. Here, using a global storm-resolving model that accurately simulates MCSs, we conclude contrasting responses to increased SST in their occurrence, that is, notable decreases over land but increases over ocean. This land-ocean contrast is attributed to the changes in convective available potential energy (CAPE) and convective inhibition (CIN). Over land, notable rises in CIN alongside moderate increases in CAPE effectively suppress (favor) weak to moderate (intense) MCSs, resulting in an overall reduction in MCS occurrences. In contrast, substantial increases in CAPE with minimal changes in CIN over ocean contribute to a significant rise in MCS occurrences. The divergent response in MCS occurrence has profound impacts on both mean and extreme precipitation.

Plain Language Summary Mesoscale convective systems (MCSs) account for more than half of tropical total rainfall and are the primary drivers of extreme rainfall and flooding events. However, understanding how the frequency of these systems will change in a warming climate remains a challenge. This is due to both the incomplete representation of these disturbances in global climate models and a lack of fundamental theory to explain their dynamics. In this study, we employ a global storm resolving model to shed light on the response of tropical MCS occurrences to climate warming. What emerges is a striking contrast: MCSs over tropical land are projected to decrease in frequency, while their occurrence over tropical oceans is anticipated to rise. This difference is linked to the relative changes in convective available potential energy and convective inhibition. The divergent response in MCS occurrences has significant implications for both average and extreme precipitation patterns. As a result, it presents challenges for developing regional climate adaptation and mitigation strategies in the face of a warming climate.

Key Points:

- A global storm resolving model is employed to study the response of global mesoscale convective systems (MCSs) to a warming climate
- Tropical MCS occurrence exhibits divergent responses to increased SST, declining over land while increasing over the ocean
- This land-ocean contrast is attributed to the changes in convective available potential energy and convective inhibition, on MCSs

Supporting Information:

Supporting Information may be found in the online version of this article.

Correspondence to:

W. Dong,
Wenhao.Dong@noaa.gov

Citation:

Dong, W., Zhao, M., Harris, L., Cheng, K.-Y., Zhou, L., & Ramaswamy, V. (2024). Contrasting response of mesoscale convective systems occurrence over tropical land and ocean to increased sea surface temperature. *Geophysical Research Letters*, *51*, e2024GL109251. https://doi.org/10.1029/2024GL109251

Received 13 MAR 2024
Accepted 31 AUG 2024
Corrected 16 NOV 2024

This article was corrected on 16 NOV 2024. See the end of the full text for details.

Author Contributions:

Conceptualization: Wenhao Dong
Data curation: Wenhao Dong, Lucas Harris, Kai-Yuan Cheng
Formal analysis: Wenhao Dong
Investigation: Wenhao Dong, Kai-Yuan Cheng
Methodology: Wenhao Dong, Ming Zhao
Resources: Wenhao Dong, Lucas Harris, Kai-Yuan Cheng
Software: Wenhao Dong

1. Introduction

Mesoscale convective systems (MCSs) play vital roles in the Earth's atmospheric circulation and the global hydrological cycle (Houze, 2004, 2018; Laing and Fritsch, 1997, 2000; Maddox, 1980; B. E. Mapes and Houze, 1993; Roca et al., 2014; Tao & Chern, 2017; Yuan & Houze, 2010). Comprehending and faithfully simulating MCSs and their responses to global warming are of paramount importance for both weather forecasting and climate projection, as they have significant implications for regional and global precipitation patterns, the occurrence of extreme weather events, and climate variability. While finer resolution (<100 km) global climate models (GCMs) have shown promising capabilities in simulating certain features of observed MCSs features, they still struggle to fully resolve the mesoscale circulation (Dong et al., 2021, 2023; Feng, Song, et al., 2021; Zhao, 2022). The current scale-separation assumptions used in GCM's deep convection parameterizations, where small cumulus scales are distinguished from the large-scale motions, fail to accurately represent the mesoscale dynamics exhibited by MCSs (Donner, 1993; Donner et al., 2001; Mapes et al., 2006; M. W. Moncrieff, 2004; M. W. Moncrieff and Liu, 2006). Although efforts have been made to address this gap by using schemes such as the Multiscale Coherent Structures Parameterization (MCSP) scheme (M. Moncrieff, 2019; Moncrieff et al., 2017) or multiscale modeling framework (MMF), also known as super-parameterization (Grabowski & Smolarkiewicz, 1999), their results have shown limited improvement in simulating observed MCSs features, leading to persistent biases in simulating various aspects of rainfall variability (Lin et al., 2017,

Supervision: Wenhao Dong
Validation: Wenhao Dong, Ming Zhao
Visualization: Wenhao Dong
Writing – original draft: Wenhao Dong
Writing – review & editing: Wenhao Dong, Ming Zhao, Lucas Harris, Kai-Yuan Cheng, Linjiong Zhou, V. Ramaswamy

2019, 2022; Xie et al., 2020; Yang et al., 2017). Consequently, many future projections of MCSs in GCMs rely on indirect analysis of their favorable large-scale conditions (Song et al., 2022; Yang et al., 2023).

Advancements in computational resources have enabled the utilization of convection-permitting models (CPMs) that operate on horizontal grids with resolutions of a few kilometers. Regional CPMs have demonstrated the ability to capture important characteristics of MCSs (Feng et al., 2018; Li et al., 2023; Prein et al., 2017a, 2020; Rasmussen et al., 2020). This increases the fidelity in the projected MCSs in a warmer climate. However, these studies have focused on limited regions (Liu et al., 2017; Prein, Rasmussen, Ikeda, et al., 2017) and employed different methods, making it challenges in comparing and interpreting their outcomes. The emergence of global CPMs, also called global storm resolving models (GSRMs), has further enhanced the representation of global cloud and convection (Satoh et al., 2019; Stevens et al., 2019). These models provide finely detailed and physically consistent simulations that extend seamlessly across various scales, eliminating the need for lateral boundary conditions and addressing the spin-up of convective features. Moreover, these models provide consistent global simulations, facilitating systematically analysis of MCSs features. GSRMs from the DYAMOND (DYnamics of the Atmospheric general circulation Modeled On Non-hydrostatic Domains) winter project (Phase-II) have been used to evaluate the representation of MCSs in the current climate. While the simulated features vary across models, they demonstrate notable improvement compared to GCMs with parameterized convection and coarser grid spacing (Feng et al., 2023).

As one of the DYAMOND GSRMs, the GFDL X-SHiELD model demonstrates reasonable simulation of various MCS characteristics, including the number of MCSs, diurnal cycle, duration, size, translation speed, as well as the associated precipitation features (Feng et al., 2023). However, this analysis is limited to 28 days (February 2020), which may introduce potential biases due to the small sample size and the focus solely on the winter season. Besides, warming scenario simulations based on GSRMs are not currently available. To address this gap, we conduct two 2-year simulations using the GFDL X-SHiELD model to systematically analyze MCSs in both present and warming climates. We begin by evaluating the present climate simulation through comparisons with satellite observations. We then investigate the effects of increased SST on MCS characteristics and associated precipitation changes using the warming simulations. To understand the potential drivers of changes in MCSs, we examine various environmental factors that influence their occurrence. To the best of our knowledge, our analysis marks the first investigation of the response of global MCSs to a warmer climate using a GSRM.

2. Materials and Methods

2.1. X-SHiELD Model Simulations

X-SHiELD is a configuration of the System for High-Resolution Prediction on Earth-to-Local Domains (SHiELD; Harris et al., 2020), which utilizes a discretized C3072 (3.25 km) cubed-sphere grid. Details of model setup are summarized in Text S1 in Supporting Information S1. A pair of experiments from the 2021 version of the X-SHiELD model are used in this study: one present-day (PD) simulation and one warming [a plus 4K (P4K)] simulation. Both simulations employ the same model configuration, with the exception that the SST in the P4K experiment is uniformly increased by 4 K globally. The duration of both runs is about 25 months, starting at 00UTC on 20 October 2019, and the analysis presented in this study covers a two-year period from January 2020 to December 2021.

2.2. Observational Data Sets

The half-hourly NASA globally merged (60°S–60°N) 4-km pixel-resolution infrared brightness temperature (T_b) data set (Janowiak et al., 2001) is used to identify and track the observed MCSs. The half-hourly NASA Integrated Multi-satellitE Retrievals for Global Precipitation Measurement (GPM/IMERG V06; Huffman et al., 2015) precipitation data set ($0.1° \times 0.1°$) is used to explore the MCS-related precipitation. Please note, as of the writing of this paper, the IMERG V06 final run product is not available after 2021/09. We use the IMERG late run product during 2021/10–2021/12. While slight differences may be present in certain grids between these two products, primarily due to additional calibration processes applied to the final run product, our findings remain consistent even when excluding the last 3 months of data. To facilitate a model-observation comparison, all observational data sets are averaged to 3-hr intervals and are remapped to match the X-SHiELD grid using the conserve method using the first-order conserve method, which preserves area-weighted averages across resolutions.

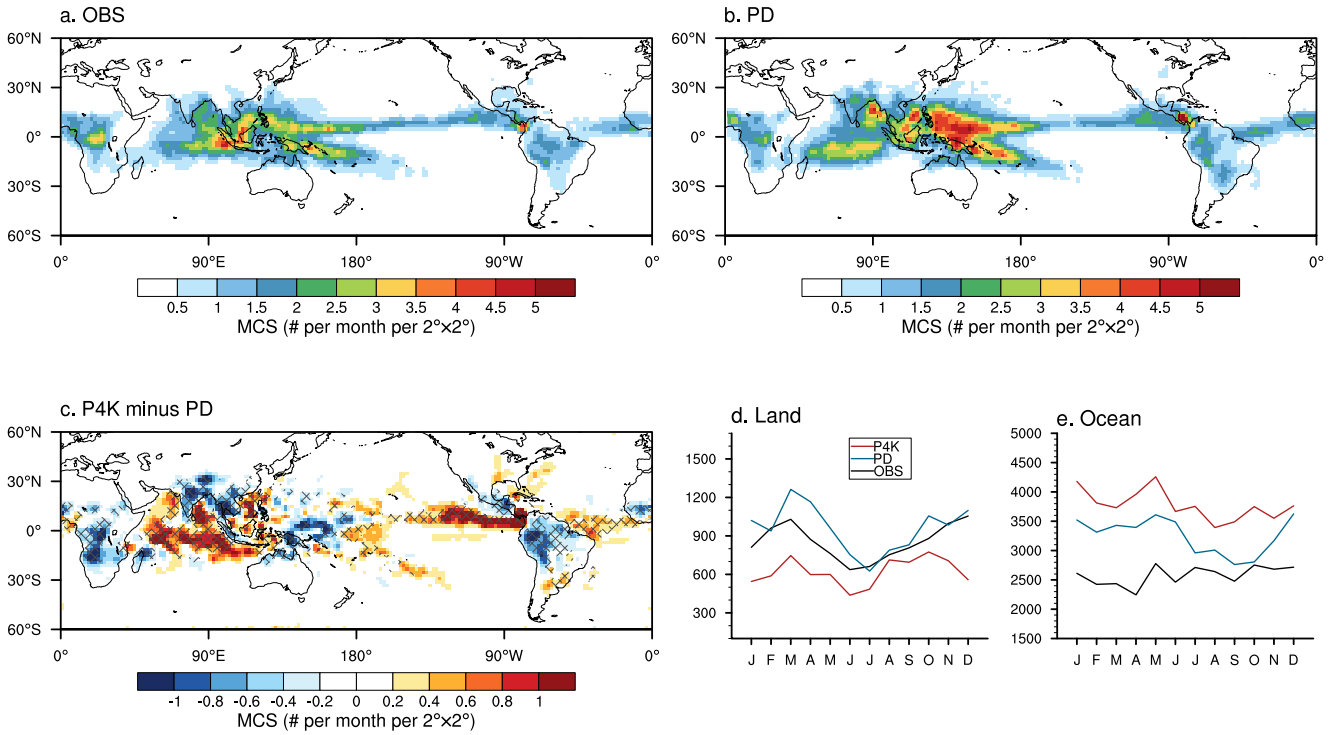

Figure 1. Spatial distribution of annual mean occurrence frequency of mesoscale convective systems (MCSs) (units: # per 2° × 2° grid) from (a) NASA observations and (b) the PD simulation. (c) The difference in the annual mean occurrence frequency of MCSs between the P4K and PD simulations. Hatchings indicate regions with differences greater than 20% relative to the PD simulation. (d)–(e) The 2-year mean seasonal occurrence frequency of MCSs based on NASA observations (black), PD simulation (blue), and P4K simulation (red) over tropical (20°S–20°N) land and ocean, respectively.

2.3. MCS Detection and Tracking Algorithm

The detection and tracking of MCSs in this study follow the approach described in Dong et al. (2021), which relies on two criteria, that is, the T_b threshold and a minimum area coverage threshold. The simulated T_b in X-SHiELD is derived from the *OLR* using methods established in our previous works (Dong et al., 2021, 2022; Zhao, 2022). As shown in Figure S1 in Supporting Information S1, the simulated mean T_b agrees well with the NASA T_b observations, with the centered pattern correlations larger than 0.98 ($p < 0.001$). The details of the tracking algorithm are outlined in Text S2 in Supporting Information S1.

3. Results

3.1. Observed and Simulated MCS Features in Current Climate

The global distribution of observed and simulated annual mean occurrence frequency of MCS is depicted in Figures 1a and 1b. Consistent with many other observational studies (Dong et al., 2020; Feng, Leung, et al., 2021; Huang et al., 2018), MCSs exhibit higher annual mean occurrence frequencies over tropical oceans. Over land, Africa, South America, and the Maritime Continent are three major regions characteristic of intensive MCS activities. The model generally captures the observed spatial distribution of the annual mean frequency of MCS, but it overestimates the frequency over the Western Pacific and Indian Ocean (Figure 1b). This overestimation aligns with biases shown in the T_b field (Figure S1c in Supporting Information S1) and is also evident in the mean precipitation pattern (Cheng et al., 2022; Harris et al., 2023). The latter has been attributed to a possible excess of shallow convective systems in these regions. In terms of its seasonal cycle, both the observation and model exhibit two peaks, typically occurring around March and December, over land regions (Figure 1d). Conversely, the seasonal evolution of MCS occurrence appears to be relatively stable when averaged over oceans (Figure 1e). The model consistently overestimates MCS frequency over oceans year-round, while its performance over land shows both positive and negative biases of smaller magnitude. While these biases may raise questions about the validity

of the projections, it is important to note that they are considerably smaller than those observed in the GCM (Dong et al., 2021) and other GSRM simulations (Feng et al., 2023).

Moreover, on an event basis, the model generally captures the observed probability distribution of MCS duration, size, and intensity (measured by the difference of mean T_b from 221 K) in the current climate for both land and ocean (Figure S2 in Supporting Information S1). Notably, observed land-based MCSs exhibit shorter durations (13.5 vs. 21.0 hr) and smaller sizes (10.3 vs. 11.1×10^4 km^2) than their oceanic counterparts; however, they are characterized by slightly stronger intensities (9.4 vs. 8.9 K). The model successfully reproduces these disparities between land and ocean, though the simulated intensity contrast is relatively smaller. Nevertheless, unlike large disparities observed in GCM simulations with conventional convective parametrization (e.g., Dong et al., 2021), the results derived from GSRM emphasize the model's reliability in simulating MCSs, thereby enhancing our confidence in its utility for exploring future MCS projections.

3.2. Response of MCS to Increased SST

When comparing the P4K with PD simulation, on average, there is a 4.5% (about 1% when normalized by the global mean change in surface temperature) increase in MCS occurrence frequency over tropical regions, defined as the area between 20°S and 20°N where MCSs are most frequent (Figure 1c). Notably, extending the tropical region to 30° S/N does not alter the results. However, these changes exhibit opposite signs over land and ocean. Specifically, MCS occurrence frequency decreases over large parts of land regions, whereas it increases over most ocean regions, except for a few small areas in the western Pacific and southwest tropical Indian Ocean. The percentage changes in MCS occurrence frequency over tropical land and ocean are −7.0% and 3.7% per degree warming, respectively. These results are qualitatively consistent with previous global and/or regional studies conducted using GCMs or regional CPMs (Dong et al., 2021; Rehbein & Ambrizzi, 2023; Zhao, 2022), although the quantitative values differ. This indicates the overall response of MCS to a warming climate is quite robust and consistent in the GSRM. Moreover, such land-ocean contrasts generally hold across all four seasons but exhibit greater complexity as one transitions from one season to another (Figure S3 in Supporting Information S1). Concerning the MCS basic features, the duration of MCSs over land and ocean has reduced slightly in the warming climate, but both their size and intensity increases (see values in Figure S2 in Supporting Information S1).

3.3. Influencing Factors for the Contrasting Response Over Land and Ocean

The contrasting responses between land and ocean in MCS occurrence frequency highlight the regional specific nature of MCS behavior in the context of a warming climate. These differences may be influenced by various factors. Prior studies have used many convective environmental proxies, including but not limited to 500-hPa vertical velocity (ω500), 0–6 km wind shear (shear06), storm relative helicity (SRH), convective available potential energy (CAPE), and convective inhibition (CIN), to investigate the impact of increased SST on convective activities (Cheng et al., 2022; Prein, 2023; Rasmussen et al., 2020). These indices in PD simulation have been evaluated in our previous works (Cheng et al., 2022; Harris et al., 2023). The model overall replicates the observed distribution and long-term averages of these indices, albeit with some variations in their absolute values [refer to Figure 3 in Cheng et al. (2022) and Figure 7 in Harris et al. (2023)].

However, their differences between P4K and PD simulations, as summarized in Figure 2, do not align with the projected changes in MCS occurrence frequency shown in Figure 1c. Notably, the spatial distribution of changes in ω500, shear06, and SRH mirrors the response of the large-scale circulation pattern to increased SST (Cheng et al., 2022; Tamarin & Kaspi, 2017; Vecchi & Soden, 2007), displaying no pronounced distinctions between land and ocean. Such inconsistencies suggest that these metrics are insufficient to account for the observed changes in MCS occurrence frequency. By contrast, CAPE and CIN show more regional specific responses to increased SST. CAPE primarily increases over the tropical oceans with large increases seen in the ITCZ and the western Pacific, while it exhibits modest changes over tropical land. Conversely, CIN intensifies predominantly over tropical land with minimal changes over oceans. These alterations have the potential to drive the divergent responses of MCS occurrence over land and ocean to increased SST.

We examine the joint probability distribution of CAPE and CIN over both tropical land and ocean where MCSs frequently occur, defined as the monthly value exceeding 0.5 per 2° × 2° grid (refer to Figure 1). This masking ensures that CAPE and CIN values relevant to convective systems are included. As shown in Figure 3, in the

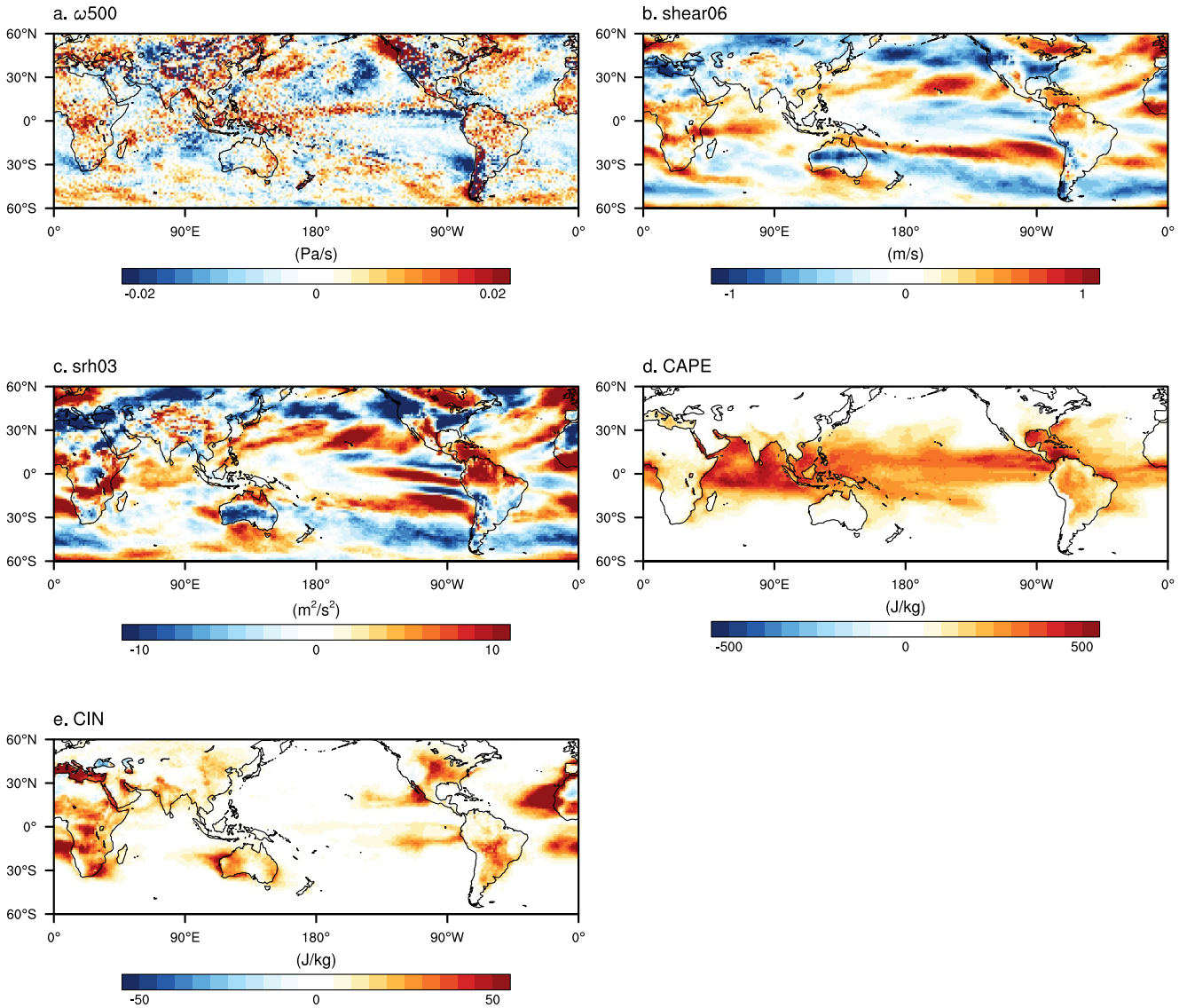

Figure 2. Spatial distribution of the annual mean (a) 500 hPa vertical velocity, (b) 0–6 km vertical wind shear, (c) 0–3 km storm-relative helicity, (d) convective available potential energy, and (e) convective inhibition between the P4K and PD simulations.

current climate, small CAPE (<1000 J kg^{-1}) and/or modest CIN (<100 J kg^{-1}) events predominant over tropical land, with their frequency decreasing as CAPE and CIN increase. By contrast, the highest frequency over tropical oceans is characterized by a border range of CAPE (300∼1500 J kg^{-1}) alongside much smaller CIN (<20 J kg^{-1}). Increased SST generally yields a broadening of the joint distribution but with a reduced gradient over both tropical land and ocean. Specifically, events with small CAPE (<500 J kg^{-1}) or small CIN (<20 J kg^{-1}) in combination with small to medium CAPE (500∼1000 J kg^{-1}) over land are projected to decrease substantially. Conversely, other events are projected to increase, albeit to a lesser extent. Similarly, the rightward shift of the distribution over tropical oceans results in a significant decrease for smaller CAPE (<1500 J kg^{-1}) cases but a notable increase in cases with higher CAPE values. These findings corroborate previous studies conducted using both coarser GCM (∼100 km) and regional CRM (∼4 km) simulations (Chen et al., 2020; Rasmussen et al., 2020).

In the warming climate, the increase in CIN contributes significantly to a decrease in MCS occurrences with lower CAPE values, which are more populated over tropical land. Concurrently, it also promotes the formation of more intense MCSs, albeit representing a smaller fraction of events, characterized by relatively larger CIN and CAPE values. These findings align with previous studies (Chen et al., 2020; Rasmussen et al., 2020), indicating that

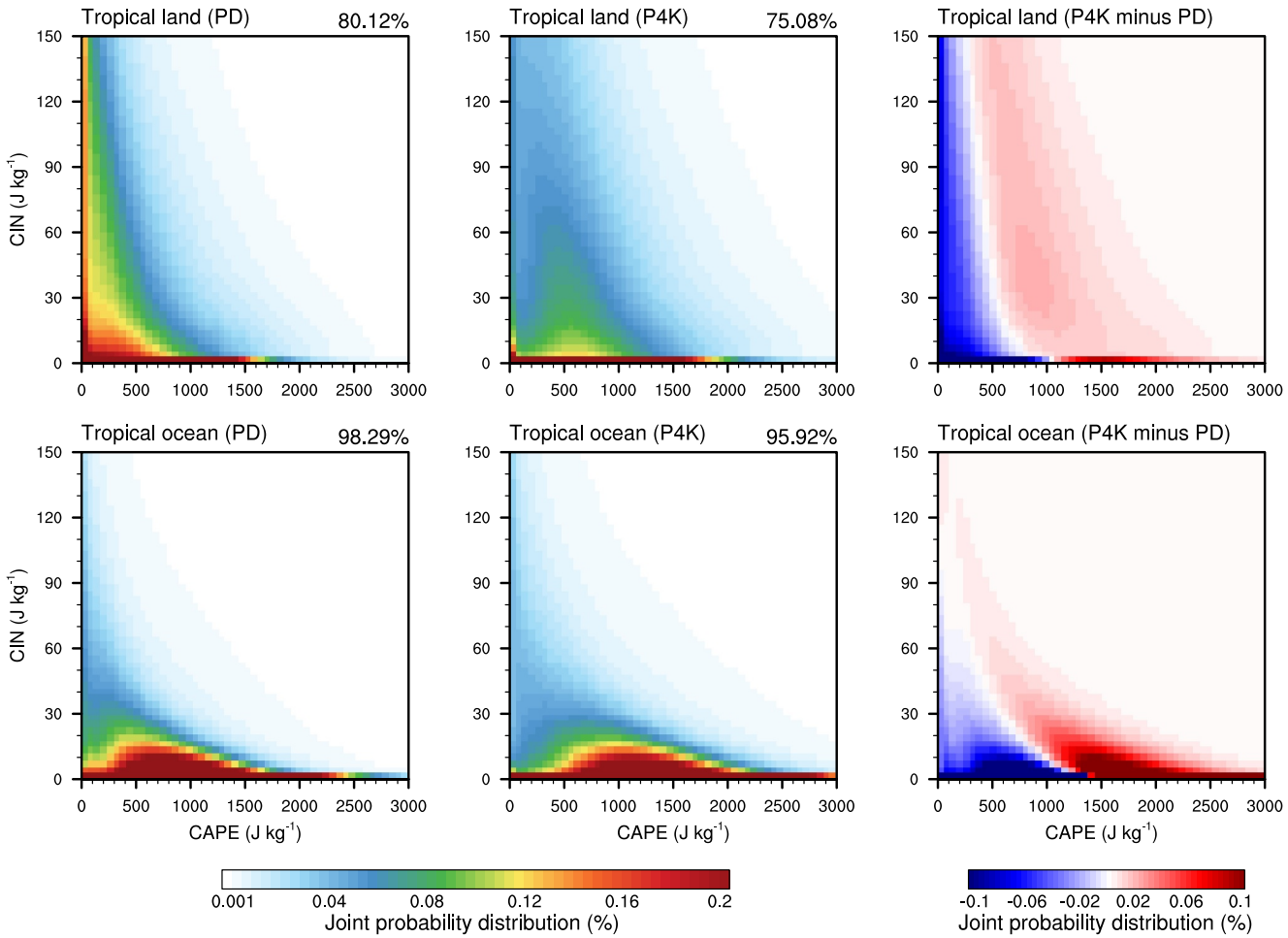

Figure 3. Joint probability distribution (units: %) of CAPE (*x*-axis) and CIN (*y*-axis) over tropical land (*upper row*) and tropical ocean (*bottom row*) in PD simulation (left), P4K simulation (middle), and their differences (right) from all convective samples. The total frequency across all bins ($0 < \text{CAPE} < 3000$ J kg^{-1}, $0 < \text{CIN} < 150$ J kg^{-1}) is displayed in the top right corner of each panel.

elevated CIN levels can influence the convective population by suppressing weaker to moderate convection while allowing larger CAPE to accumulate to higher levels, potentially leading to more frequent severe convective events. Similarly, over tropical oceans, the substantial increase in CAPE, accompanied by minimal changes in CIN, leads to an overall increase in MCS occurrences. This is consistent with previous theoretical and modeling studies, which suggest that the rise in CAPE alone in a warming climate could lead to more convective events (Muller & Takayabu, 2020). These patterns persist when analyzing CAPE-CIN associated with individual MCS event (Figure S4 in Supporting Information S1), though the high-frequency center of the joint distributions, over both land and ocean, shifts toward higher CIN values. This deviation toward relatively larger CIN values underscores the crucial role of CIN in shaping the dynamics of intense convective events. This is possibly because intense convection, such as MCSs, benefits from a buildup of instability, where higher CIN values can prevent premature convection, allowing instability to accumulate. The contrasting response of CAPE and CIN to increased SST originates from different changes in low-level temperature and humidity (i.e., relative humidity) with global warming. Consistent with previous studies (Chen et al., 2020), the increase in CAPE over the tropical ocean depends heavily on low-level humidity, which is driven more by temperature increase as relative humidity remains nearly constant over the ocean (Figure S5a in Supporting Information S1). By contrast, the increase in CIN over tropical land is largely affected by the reduction in low-level relative humidity (Figure S5b in Supporting Information S1).

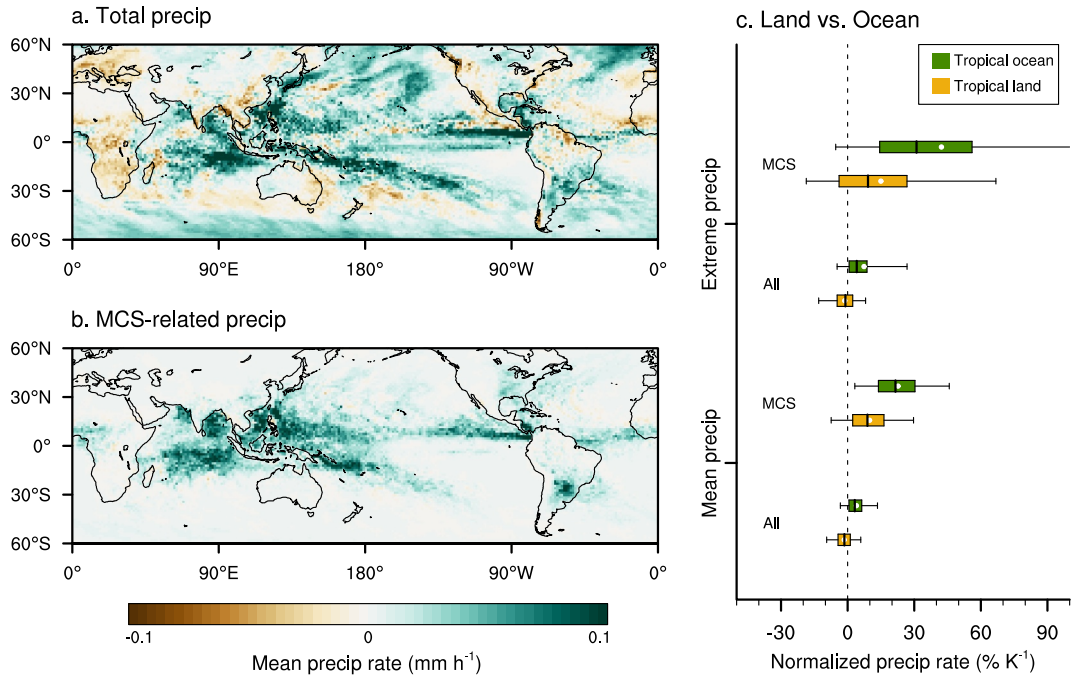

Figure 4. Differences in mean precipitation rate (units: mm h^{-1}) of (a) total precipitation, (b) MCS-associated precipitation between the PD and P4K simulations. (c) Boxplot of the normalized changes in precipitation rate (units: % K^{-1}) between the PD and P4K simulations for mean and extreme precipitation, including both total and MCS-related over tropical land and ocean. The boxes indicate 5%-quantile, 25%-quantile, median, 75%-quantile, and 95%-quantile, respectively. White dots represent the corresponding means.

3.4. Impact on Mean and Extreme Precipitation Pattern

As a highly efficient rain-producing system, changes in MCS occurrences are expected to have a profound impact on precipitation patterns. Precipitation associated with MCSs contributes to around 50% of total precipitation in many parts of the tropics (Figure S6 in Supporting Information S1). The model generally reproduces the spatial distribution, but notably underestimates the portion over the ocean, particularly in the West Pacific. This discrepancy primarily stems from the excessive total precipitation generated by the model (Harris et al., 2023). On an event basis, the simulated mean and total precipitation volume within each MCS are biased low compared to observations (Figure S2 in Supporting Information S1). These biases arise mainly from the model's tendency to produce broader areas of lighter precipitation (Harris et al., 2023).

As a response to uniform SST warming, substantial increases in mean precipitation are projected over large parts of tropical ocean (>75%), where higher MCS occurrences are expected (Figure 4a). Conversely, approximately 65% tropical land region, where fewer MCSs are projected, experiences reductions in mean precipitation. When normalized by the global mean change in surface temperature, the mean precipitation rate averaged over tropical land decreases by 1.5% K^{-1} but increases by 3.9% K^{-1} when averaged over tropical ocean (Figure 4c). This difference mainly reflects the changes in MCS occurrence frequency, as the majority of MCS-related precipitation rate over both tropical land and ocean exhibits larger increasing rates (Figure 4b). The average normalized change rate of MCS-associated precipitation over tropical land is about 9.9% K^{-1}, while it is 22.7% K^{-1} over tropical ocean (Figure 4c). Within each MCS, the normalized rate of MCS-associated precipitation increases by 28.7% K^{-1} over tropical land, while it increases by 18.1% K^{-1} over tropical ocean (Figure S2 in Supporting Information S1). The increasing rate of total precipitation volume within each MCS is higher over land (1.9% K^{-1}) than over ocean (1.4% K^{-1}), likely due to the combined effects of a larger increase in mean precipitation rates and MCS sizes (Figure S2 in Supporting Information S1). The skewness of precipitation within each MCS, although biased large in the present climate, decreases as climate warms, indicating that precipitation associated with MCSs may become more dispersed around the center of the systems, potentially affecting a larger area.

In addition, MCSs also play a pivotal role in triggering extreme rainfall and flooding events in tropical regions (Cheng et al., 2023; Dong et al., 2021; Houze, 2018; Prein et al., 2023). We examine the changes in the frequency of precipitation extremes, defined as the 95th percentile of all precipitation samples for each grid. The results remain consistent when the 90th percentile is utilized. The model well captures the magnitude of the precipitation extremes (Figure S7 in Supporting Information S1), and effectively reproduces the observed spatial distribution (Figure S8 in Supporting Information S1). The projected changes in precipitation extremes mirror the changes in total precipitation. When attributed to MCSs, there are significant increases in precipitation extremes over both tropical land and ocean (Figure 4c and Figure S9 in Supporting Information S1). Our results are consistent with Guendelman et al. (2024), who used the same simulations. Despite the use of daily precipitation data, they found that mean precipitation over tropical land will decrease at a similar rate as reported here. However, when precipitation is categorized into different percentiles, the response of land precipitation to warming shows a decrease for small and moderate rates but an increase for higher rates, likely related to MCSs.

4. Conclusions

Despite the critical role of MCS in the tropical climate, our understanding of their future behavior remains incomplete. In this study, we demonstrated the success of a GSRM in simulating the observed MCS features and revealed contrasting projections for tropical land and ocean MCS occurrence in a warming environment. These patterns persist despite the seasonal variations. A comprehensive analysis of multiple convection-relevant environmental factors indicates that the divergent responses in MCS occurrence are closely linked to changes in CAPE and CIN. Over tropical land, while CAPE exhibits minor increases, CIN experiences a significant rise. The increased CIN effectively suppresses weaker to moderate MCSs, yet it facilitates the accumulation of larger CAPE values, resulting in more frequent intense MCS events. The dual influence leads to an overall reduction in MCS occurrences over tropical land. In contrast, over tropical oceans, CAPE is projected to largely increase while CIN shows minimal changes. The dominant role played by the increasing CAPE contributes to an overall increase in MCS occurrences.

The contrasting response of MCS occurrence over tropical land and ocean significantly influences tropical precipitation patterns. While the positive bias in MCS occurrence simulated over the western Pacific and the large biases in MCS associated precipitation may raise questions about the validity of the projections, it's worth noting that these biases are considerably smaller than that observed in the GCM and other GSRM simulations (Dong et al., 2021; Feng et al., 2023). Therefore, our analysis may hold greater relevance for understanding future changes in MCS features and the associated precipitation patterns. However, the simulated land-ocean contrast in the intensity of MCSs is relatively weaker when compared to observations and other GSRM simulations. Additionally, it's important to acknowledge that the P4K experiment did not include a CO_2 increase or SST pattern change, potentially affecting the direct radiative effect of CO_2 and variability in SST on MCS responses to warming. Furthermore, uncertainties in future projections may arise due to model deficiencies in simulating the current climate. Lastly, while CAPE and CIN are shown to be useful in explaining MCS changes, their specific roles in MCS initiation and throughout its lifecycle remain unexplored. Their interactions with other influencing factors may also play a significant role. A more rigorous analysis of this paradigm using idealized/limited domain simulations would provide valuable insights. Nonetheless, the expansion of MCS size, intensification of its intensity and the associated precipitation extremes present a significant threat to tropical populations, underscoring the critical need to develop effective strategies for adaptation and mitigation in the face of a changing climate.

Data Availability Statement

All data are available in the main text or the supplementary materials. The half-hourly NASA globally merged 4-km pixel-resolution infrared brightness temperature data set can be downloaded from https://disc2.gesdisc.eosdis.nasa.gov/data/MERGED_IR/GPM_MERGIR.1/. The half-hourly NASA Integrated Multi-satellitE Retrievals for Global Precipitation Measurement (GPM/IMERG V06) final run product for the period 2020/01–2021/09 can be downloaded from https://gpm1.gesdisc.eosdis.nasa.gov/data/GPM_L3/GPM_3IMERGHH.07/, while the late run product for 2021/10–2021/12 can be downloaded from https://gpm1.gesdisc.eosdis.nasa.gov/data/GPM_L3/GPM_3IMERGHHL.06/. Please be aware of the recent updates to the GPM/IMERG V06 and V07 products (https://gpm.nasa.gov/mission/news/status-imerg-version-06-and-07-data). Public releases of SHiELD are accessible at https://github.com/NOAA-GFDL/SHiELD_build. The code used for the version of X-SHiELD in

this paper is available in Harris et al. (2023). All custom codes are direct implementation of standard methods and techniques, described in details in Materials and Methods. The X-SHiELD simulations for the year 2021 are available through the NOAA Open Data Dissemination (NODD) on Google Cloud (https://console.cloud.google.com/storage/browser/gfdl-xshield-pire-2022). The processed monthly data sets from X-SHiELD simulations for the years 2020–2021 used in this study have been archived on Zenodo (W. Dong, 2024).

Acknowledgments
The authors would like to thank L. Donner, T. Abbott, Z. Tan, P. Lin, T. Merlis, and Y. Kuo for the useful discussions and comments on earlier versions of this paper. The authors are also grateful to S. Clark for providing the information about the coarse graining method implemented in X-SHiELD. This research from the Geophysical Fluid Dynamics Laboratory is supported by NOAA's Science Collaboration Program and administered by UCAR's Cooperative Programs for the Advancement of Earth System Science (CPAESS) under awards NA16NWS4620043 (to W.D.) and NA18NWS4620043B (to W.D.). Cheng is supported under awards NA18OAR4320123, NA19OAR0220146, and NA19OAR0220147 from NOAA. Cheng is additionally supported under the NOAA Research Global-Nest initiative.

References

Chen, J., Dai, A., Zhang, Y., & Rasmussen, K. L. (2020). Changes in convective available potential energy and convective inhibition under global warming. *Journal of Climate*, *33*(6), 2025–2050. https://doi.org/10.1175/jcli-d-19-0461.1

Cheng, K. Y., Harris, L., Bretherton, C., Merlis, T. M., Bolot, M., Zhou, L., et al. (2022). Impact of warmer Sea Surface temperature on the global pattern of intense convection: Insights from a global storm resolving model. *Geophysical Research Letters*, *49*(16), e2022GL099796. https://doi.org/10.1029/2022gl099796

Cheng, Y. M., Dias, J., Kiladis, G., Feng, Z., & Leung, L. R. (2023). Mesoscale convective systems modulated by convectively coupled equatorial waves. *Geophysical Research Letters*, *50*(10), e2023GL103335. https://doi.org/10.1029/2023gl103335

Dong, W. (2024). Processed monthly datasets from X-SHiELD simulations. [Dataset]. *Zenodo*. https://doi.org/10.5281/zenodo.12522150

Dong, W., Zhao, M., Ming, Y., Krasting, J. P., & Ramaswamy, V. (2023). Simulation of United States mesoscale convective systems using GFDL's new high-resolution general circulation model. *Journal of Climate*, *36*(19), 6967–6990. https://doi.org/10.1175/jcli-d-22-0529.1

Dong, W., Zhao, M., Ming, Y., & Ramaswamy, V. (2021). Representation of tropical mesoscale convective systems in a general circulation model: Climatology and response to global warming. *Journal of Climate*, *34*(14), 5657–5671.

Dong, W., Zhao, M., Ming, Y., & Ramaswamy, V. (2022). Significant increase in Sea Surface temperature at the genesis of tropical mesoscale convective systems. *Geophysical Research Letters*, *49*(24), e2022GL101950. https://doi.org/10.1029/2022gl101950

Dong, W. H., Lin, Y. L., Zhang, M. H., & Huang, X. M. (2020). Footprint of tropical mesoscale convective system variability on stratospheric water vapor. *Geophysical Research Letters*, *47*(5), e2019GL086320. https://doi.org/10.1029/2019gl086320

Donner, L. J. (1993). A cumulus parameterization including mass fluxes, vertical momentum dynamics, and mesoscale effects. *Journal of the Atmospheric Sciences*, *50*(6), 889–906. https://doi.org/10.1175/1520-0469(1993)050<0889:acpimf>2.0.co;2

Donner, L. J., Seman, C. J., Hemler, R. S., & Fan, S. M. (2001). A cumulus parameterization including mass fluxes, convective vertical velocities, and mesoscale effects: Thermodynamic and hydrological aspects in a general circulation model. *Journal of Climate*, *14*(16), 3444–3463. https://doi.org/10.1175/1520-0442(2001)014<3444:acpimf>2.0.co;2

Feng, Z., Leung, L. R., Hardin, J., Terai, C. R., Song, F., & Caldwell, P. (2023). Mesoscale convective systems in DYAMOND global convection-permitting simulations. *Geophysical Research Letters*, *50*(4), e2022GL102603. https://doi.org/10.1029/2022gl102603

Feng, Z., Leung, L. R., Houze, R. A., Jr., Hagos, S., Hardin, J., Yang, Q., et al. (2018). Structure and evolution of mesoscale convective systems: Sensitivity to cloud microphysics in convection-permitting simulations over the United States. *Journal of Advances in Modeling Earth Systems*, *10*(7), 1470–1494. https://doi.org/10.1029/2018ms001305

Feng, Z., Leung, L. R., Liu, N., Wang, J., Houze, R. A., Jr., Li, J., et al. (2021). A global high-resolution mesoscale convective system database using satellite-derived cloud tops, surface precipitation, and tracking. *Journal of Geophysical Research: Atmospheres*, *126*(8), e2020JD034202. https://doi.org/10.1029/2020jd034202

Feng, Z., Song, F., Sakaguchi, K., & Leung, L. R. (2021). Evaluation of mesoscale convective systems in climate simulations: Methodological development and results from mpas-cam over the United States. *Journal of Climate*, *34*(7), 2611–2633. https://doi.org/10.1175/jcli-d-20-0136.1

Grabowski, W. W., & Smolarkiewicz, P. K. (1999). Crcp: A cloud resolving convection parameterization for modeling the tropical convecting atmosphere. *Physica D: Nonlinear Phenomena*, *133*(1–4), 171–178. https://doi.org/10.1016/s0167-2789(99)00104-9

Guendelman, I., Merlis, T. M., Cheng, K. Y., Harris, L. M., Bretherton, C. S., Bolot, M., et al. (2024). The precipitation response to warming and CO_2 increase: A comparison of a global storm resolving model and CMIP6 models. *Geophysical Research Letters*, *51*(7), e2023GL107008. https://doi.org/10.1029/2023gl107008

Harris, L., Zhou, L., Kaltenbaugh, A., Clark, S., Cheng, K. Y., & Bretherton, C. (2023). A global survey of rotating convective updrafts in the GFDL X-SHiELD 2021 global storm resolving model. *Journal of Geophysical Research: Atmospheres*, *128*(10), e2022JD037823. https://doi.org/10.1029/2022jd037823

Harris, L., Zhou, L., Lin, S. J., Chen, J. H., Chen, X., Gao, K., et al. (2020). Gfdl SHiELD: A unified system for weather-to-seasonal prediction. *Journal of Advances in Modeling Earth Systems*, *12*(10), e2020MS002223. https://doi.org/10.1029/2020ms002223

Houze, R. A. (2004). Mesoscale convective systems. *Reviews of Geophysics*, *42*(4). https://doi.org/10.1029/2004rg000150

Houze, R. A. (2018). 100 years of research on mesoscale convective systems. *Meteorological Monographs*, *59*, 17–21. https://doi.org/10.1175/amsmonographs-d-18-0001.1

Huang, X., Hu, C., Huang, X., Chu, Y., Tseng, Y.-h., Zhang, G. J., & Lin, Y. (2018). A long-term tropical mesoscale convective systems dataset based on a novel objective automatic tracking algorithm. *Climate Dynamics*, *51*(7), 3145–3159. https://doi.org/10.1007/s00382-018-4071-0

Huffman, G. J., Bolvin, D. T., Braithwaite, D., Hsu, K., Joyce, R., Xie, P., & Yoo, S. H. (2015). NASA global precipitation measurement (GPM) integrated multi-satellite retrievals for GPM (IMERG). *Algorithm theoretical basis document (ATBD) version*, *4*(26), 30.

Janowiak, J. E., Joyce, R. J., & Yarosh, Y. (2001). A real-time global half-hourly pixel-resolution infrared dataset and its applications. *Bulletin of the American Meteorological Society*, *82*(2), 205–218. https://doi.org/10.1175/1520-0477(2001)082<0205:artghh>2.3.co;2

Laing, A. G., & Fritsch, J. M. (1997). The global population of mesoscale convective complexes. *Quarterly Journal of the Royal Meteorological Society*, *123*(538), 389–405. https://doi.org/10.1002/qj.49712353807

Laing, A. G., & Fritsch, J. M. (2000). The large-scale environments of the global populations of mesoscale convective complexes. *Monthly Weather Review*, *128*(8), 2756–2776. https://doi.org/10.1175/1520-0493(2000)128<2756:tlseot>2.0.co;2

Li, P., Song, F., Chen, H., Li, J., Prein, A. F., Zhang, W., et al. (2023). Intensification of mesoscale convective systems in the East Asian rainband over the past two decades. *Geophysical Research Letters*, *50*(16), e2023GL103595. https://doi.org/10.1029/2023gl103595

Lin, G., Fan, J., Feng, Z., Gustafson, W. I., Jr., Ma, P.-L., & Zhang, K. (2019). Can the multiscale modeling framework (MMF) simulate the MCS-associated precipitation over the central United States? *Journal of Advances in Modeling Earth Systems*, *11*(12), 4669–4686. https://doi.org/10.1029/2019ms001849

Lin, G., Jones, C. R., Leung, L. R., Feng, Z., & Ovchinnikov, M. (2022). Mesoscale convective systems in a superparameterized E3SM simulation at high resolution. *Journal of Advances in Modeling Earth Systems*, *14*(1), e2021MS002660. https://doi.org/10.1029/2021ms002660

Lin, Y., Dong, W., Zhang, M., Xie, Y., Xue, W., Huang, J., & Luo, Y. (2017). Causes of model dry and warm bias over central US and impact on climate projections. *Nature Communications*, *8*(1), 1–8. https://doi.org/10.1038/s41467-017-01040-2

Liu, C., Ikeda, K., Rasmussen, R., Barlage, M., Newman, A. J., Prein, A. F., et al. (2017). Continental-scale convection-permitting modeling of the current and future climate of North America. *Climate Dynamics*, *49*(1–2), 71–95. https://doi.org/10.1007/s00382-016-3327-9

Maddox, R. A. (1980). Mesoscale convective complexes. *Bulletin of the American Meteorological Society*, *61*(11), 1374–1387. https://doi.org/10.1175/1520-0477(1980)061<1374:mcc>2.0.co;2

Mapes, B., Tulich, S., Lin, J., & Zuidema, P. (2006). The mesoscale convection life cycle: Building block or prototype for large-scale tropical waves? *Dynamics of Atmospheres and Oceans*, *42*(1–4), 3–29. https://doi.org/10.1016/j.dynatmoce.2006.03.003

Mapes, B. E., & Houze, R. A., Jr. (1993). Cloud clusters and superclusters over the oceanic warm pool. *Monthly Weather Review*, *121*(5), 1398–1416. https://doi.org/10.1175/1520-0493(1993)121<1398:ccasot>2.0.co;2

Moncrieff, M. W. (2004). Analytic representation of the large-scale organization of tropical convection. *Journal of the Atmospheric Sciences*, *61*(13), 1521–1538. https://doi.org/10.1175/1520-0469(2004)061<1521:arotlo>2.0.co;2

Moncrieff, M. W. (2019). Toward a dynamical foundation for organized convection parameterization in GCMs. *Geophysical Research Letters*, *46*(23), 14103–14108. https://doi.org/10.1029/2019gl085316

Moncrieff, M. W., & Liu, C. (2006). Representing convective organization in prediction models by a hybrid strategy. *Journal of the Atmospheric Sciences*, *63*(12), 3404–3420. https://doi.org/10.1175/jas3812.1

Moncrieff, M. W., Liu, C., & Bogenschutz, P. (2017). Simulation, modeling, and dynamically based parameterization of organized tropical convection for global climate models. *Journal of the Atmospheric Sciences*, *74*(5), 1363–1380. https://doi.org/10.1175/jas-d-16-0166.1

Muller, C., & Takayabu, Y. (2020). Response of precipitation extremes to warming: What have we learned from theory and idealized cloud-resolving simulations, and what remains to be learned? *Environmental Research Letters*, *15*(3), 035001. https://doi.org/10.1088/1748-9326/ab7130

Prein, A. F. (2023). Thunderstorm straight line winds intensify with climate change. *Nature Climate Change*, *13*(12), 1353–1359. https://doi.org/10.1038/s41558-023-01852-9

Prein, A. F., Liu, C., Ikeda, K., Bullock, R., Rasmussen, R. M., Holland, G. J., & Clark, M. (2020). Simulating North American mesoscale convective systems with a convection-permitting climate model. *Climate Dynamics*, *55*(1), 95–110. https://doi.org/10.1007/s00382-017-3993-2

Prein, A. F., Mooney, P. A., & Done, J. M. (2023). The multi-scale interactions of atmospheric phenomenon in mean and extreme precipitation. *Earth's Future*, *11*(11), e2023EF003534. https://doi.org/10.1029/2023ef003534

Prein, A. F., Rasmussen, R., & Stephens, G. (2017). Challenges and advances in convection-permitting climate modeling. *Bulletin of the American Meteorological Society*, *98*(5), 1027–1030. https://doi.org/10.1175/bams-d-16-0263.1

Prein, A. F., Rasmussen, R. M., Ikeda, K., Liu, C., Clark, M. P., & Holland, G. J. (2017). The future intensification of hourly precipitation extremes. *Nature Climate Change*, *7*(1), 48–52. https://doi.org/10.1038/nclimate3168

Rasmussen, K. L., Prein, A. F., Rasmussen, R. M., Ikeda, K., & Liu, C. (2020). Changes in the convective population and thermodynamic environments in convection-permitting regional climate simulations over the United States. *Climate Dynamics*, *55*(1–2), 383–408. https://doi.org/10.1007/s00382-017-4000-7

Rehbein, A., & Ambrizzi, T. (2023). Mesoscale convective systems over the Amazon basin in a changing climate under global warming. *Climate Dynamics*, *61*(3–4), 1–13. https://doi.org/10.1007/s00382-022-06657-8

Roca, R., Aublanc, J., Chambon, P., Fiolleau, T., & Viltard, N. (2014). Robust observational quantification of the contribution of mesoscale convective systems to rainfall in the tropics. *Journal of Climate*, *27*(13), 4952–4958. https://doi.org/10.1175/jcli-d-13-00628.1

Satoh, M., Stevens, B., Judt, F., Khairoutdinov, M., Lin, S. J., Putman, W. M., & Düben, P. (2019). Global cloud-resolving models. *Current Climate Change Reports*, *5*(3), 172–184. https://doi.org/10.1007/s40641-019-00131-0

Song, F., Leung, L. R., Feng, Z., Chen, X., & Yang, Q. (2022). Observed and projected changes of large-scale environments conducive to spring MCS initiation over the US great plains. *Geophysical Research Letters*, *49*(15), e2022GL098799. https://doi.org/10.1029/2022gl098799

Stevens, B., Satoh, M., Auger, L., Biercamp, J., Bretherton, C. S., Chen, X., et al. (2019). Dyamond: The DYnamics of the atmospheric general circulation modeled on non-hydrostatic domains. *Progress in Earth and Planetary Science*, *6*(1), 1–17. https://doi.org/10.1186/s40645-019-0304-z

Tamarin, T., & Kaspi, Y. (2017). The poleward shift of storm tracks under global warming: A Lagrangian perspective. *Geophysical Research Letters*, *44*(20), 10–666. https://doi.org/10.1002/2017gl073633

Tao, W.-K., & Chern, J.-D. (2017). The impact of simulated mesoscale convective systems on global precipitation: A multiscale modeling study. *Journal of Advances in Modeling Earth Systems*, *9*(2), 790–809. https://doi.org/10.1002/2016ms000836

Vecchi, G. A., & Soden, B. J. (2007). Global warming and the weakening of the tropical circulation. *Journal of Climate*, *20*(17), 4316–4340. https://doi.org/10.1175/jcli4258.1

Xie, S., Leung, L.-Y., Feng, Z., Lin, W., Chen, C.-C., Richter, J., & Fan, J. (2020). *Fy2020 fourth quarter performance metric: Evaluate improvement in simulations of mesoscale convective systems from new parameterization developments in E3SM. Tech. rep*. Lawrence Livermore National Lab.(LLNL).

Yang, Q., Houze Jr, R. A., Leung, L. R., & Feng, Z. (2017). Environments of long-lived mesoscale convective systems over the central United States in convection permitting climate simulations. *Journal of Geophysical Research: Atmospheres*, *122*(24), 13–288. https://doi.org/10.1002/2017jd027033

Yang, Q., Leung, L. R., Feng, Z., & Chen, X. (2023). Impact of global warming on US summertime mesoscale convective systems: A simple Lagrangian parcel model perspective. *Journal of Climate*, *36*(14), 4597–4618. https://doi.org/10.1175/jcli-d-22-0291.1

Yuan, J., & Houze, R. A. (2010). Global variability of mesoscale convective system anvil structure from a-train satellite data. *Journal of Climate*, *23*(21), 5864–5888. https://doi.org/10.1175/2010jcli3671.1

Zhao, M. (2022). A study of AR-TS-and MCS-associated precipitation and extreme precipitation in present and warmer climates. *Journal of Climate*, *35*(2), 479–497. https://doi.org/10.1175/jcli-d-21-0145.1

References From the Supporting Information

Anderson, C. J., & Arritt, R. W. (2001). Mesoscale convective systems over the United States during the 1997–98 El Niño. *Monthly Weather Review*, *129*(9), 2443–2457. https://doi.org/10.1175/1520-0493(2001)129<2443:mcsotu>2.0.co;2

Cheeks, S. M., Fueglistaler, S., & Garner, S. T. (2020). A satellite-based climatology of central and southeastern us mesoscale convective systems. *Monthly Weather Review*, *148*(6), 2607–2621. https://doi.org/10.1175/mwr-d-20-0027.1

Han, J., & Bretherton, C. S. (2019). TKE-based moist eddy-diffusivity mass-flux (EDMF) parameterization for vertical turbulent mixing. *Weather and Forecasting*, *34*(4), 869–886. https://doi.org/10.1175/waf-d-18-0146.1

Han, J., Witek, M. L., Teixeira, J., Sun, R., Pan, H. L., Fletcher, J. K., & Bretherton, C. S. (2016). Implementation in the NCEP GFS of a hybrid eddy-diffusivity mass-flux (EDMF) boundary layer parameterization with dissipative heating and modified stable boundary layer mixing. *Weather and Forecasting*, *31*(1), 341–352. https://doi.org/10.1175/waf-d-15-0053.1

Pollard, R. T., Rhines, P. B., & Thompson, R. O. (1973). The deepening of the wind-mixed layer. *Geophysical Fluid Dynamics*, *4*(4), 381–404. https://doi.org/10.1080/03091927208236105

Zhou, L., Harris, L., Chen, J. H., Gao, K., Guo, H., Xiang, B., et al. (2022). Improving global weather prediction in GFDL SHiELD through an upgraded GFDL cloud microphysics scheme. *Journal of Advances in Modeling Earth Systems*, *14*(7), e2021MS002971. https://doi.org/10.1029/2021ms002971

Zhou, L., Lin, S. J., Chen, J. H., Harris, L. M., Chen, X., & Rees, S. L. (2019). Toward convective-scale prediction within the next generation global prediction system. *Bulletin of the American Meteorological Society*, *100*(7), 1225–1243. https://doi.org/10.1175/bams-d-17-0246.1

Erratum

The originally published version of this article contained a typographical error. The title of Section 2.1 should be changed to the following: "X-SHiELD Model Simulations." The error has been corrected, and this may be considered the authoritative version of record.